Miniaturized Fiber Interferometers and Their Applications as Fiber Sensors

Bo Dong, Banghong Zhang, Junhong Ng, and Yixin Wang
Institute for Infocomm Research (I2R), Singapore 138632, Singapore

Abstract— Recently, much attention has been focused on the miniaturized fiber interferometer devices due to their advantages of compact structure, small size and low cost. In this paper, we introduce two types of miniaturized fiber Mach-Zehnder interferometer (FMZI) and fiber Fabry-Perot interferometer (FFPI) and their applications as fiber sensors. An in line miniaturized FMZI could be fabricated by discharge or a point hydrogen flame. Here, we demonstrate its application as a fiber temperature sensor. A miniaturized FFPI could be fabricated by discharge when a hollow core photonic crystal fiber is spliced to a single mode fiber. Here, we demonstrate its application as a liquid refractive index sensor.

1. INTRODUCTION

Miniaturized fiber interferometers have attracted much attention due to their inherent advantages of small size, compact structure and low cost. Especially, they are more stable compared to the other common fiber interferometers and have been widely used in fiber sensing [1–9]. There are two main miniaturized fiber interferometers, fiber Mach-Zehnder interferometer (FMZI) and fiber Fabry-Perot interferometer (FFPI). Generally, miniaturized FMZI could be fabricated by discharge [1] or a point flame [2]. There is also the other method of just splicing a short-length multimode fiber [3] or photonic crystal fiber (PCF) between two sections of single mode fibers (SMFs) [4, 5]. Miniaturized FFPIs could be fabricated by discharge [6] or just splicing a short-length hollow core PCF between two sections of SMFs [7, 8]. To this day, miniaturized FMZIs have been widely used as fiber sensors for measuring force [3], strain [4, 5], displacement, temperature [4, 5, 9], vibration [2] and refractive index (RI), and miniaturized FFPIs have been applied to measure strain [7], pressure and RI [6].

In this paper, we demonstrate our recent research achievements in minimized FMZIs and FFPIs. An in line miniaturized FMZI could be fabricated in a short-length fiber with two abrupt-tapers by discharge or a point flame. Compared to the discharge method, a much smaller FMZI could be obtained by the point flame method. Here we demonstrate its application as fiber temperature sensor. An in line fiber miniaturized FFPI could be fabricated by discharge when splicing a hollow core PCF to an SMF. Here, we demonstrate its application as a liquid refractive index sensor.

2. MINIATURIZED FMZI AND ITS APPLICATION

To introduce a taper on the common fiber, two heating methods are generally applied, discharge and a point flame. The discharge method could fabricate the taper automatically by setting suitable splicing parameters of a splicer. The point flame could provide a higher heating temperature than the inner portion. To introduce the taper, one end of the fiber is fixed and the other end is pulled by a step motor or a suitable weight. Fig. 1(a) shows the schematic diagram of fabricating the taper. Figs. 1(b) and 1(c) show two typical types of tapers. Using the point flame method can not only get a longer, uniform and smooth fiber taper shown in Fig. 1(b) but also a much shorter abrupt taper shown in Fig. 1(c). However, using the discharge method can only get the abrupt taper, and the operation of this method is limited by the structure of the splicer.

Figure 2 shows the typical structure of an abrupt-tapered FMZI.The fundamental mode propagates in the untapered fiber, when it propagates to the left taper, corresponding core mode and high order cladding modes will be excited. When they meet at the right taper, corresponding interferences among them will occur. If the power is mainly distributed in the core mode and dominated cladding mode, the interference can approximatively be regarded as a two-beam Mach-Zehnder interference. To get an FMZI with a higher interference depth, a suitable taper waist diameter is required. Experiments show that to get the extinction ratio (ER) of more than 20-dB, generally ∼20-µm taper waist diameter of the common fiber is needed. However, for the Er/Yb co-doped fiber(EYF) based FMZI, only ∼50-µm waist diameter is needed. Fig. 3 shows the typical transmission spectrum of an EYF based FMZI and its corresponding spatial frequency spectrum. Its length is about 10.5 mm. The two tapers have waist lengths and diameters of 43.4 and 430 µm, and 56.1 and 470 μm, respectively. The distance between the two centers of the abrupt tapers is about 5 mm.

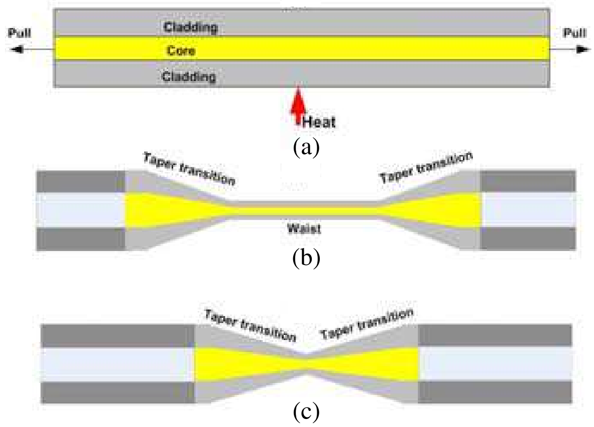

Figure 1: Schematic diagrams of two types of fiber tapers.

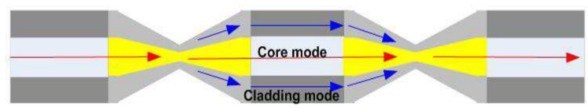

Figure 2: Schematic diagram of the FMZI.

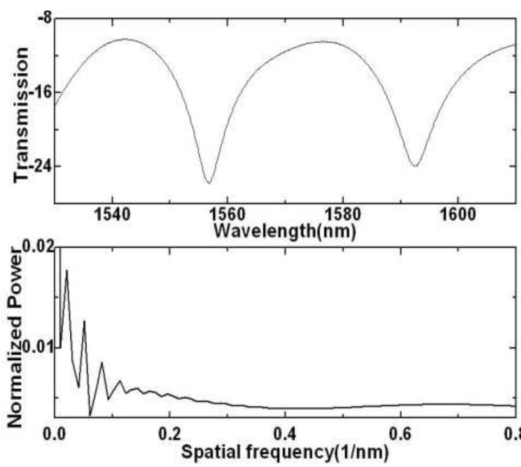

Figure 3: Typical transmission spectrom of the EYF based FMZI and its corresponding spatial frequency.

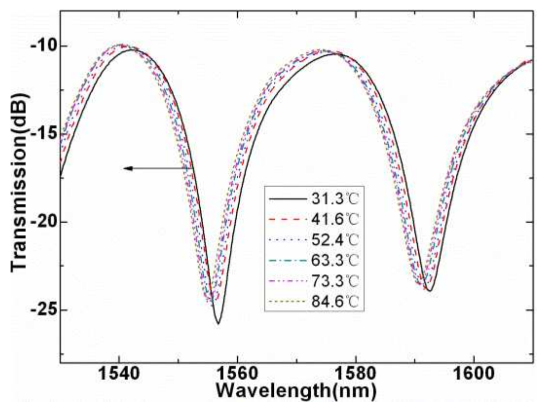

Figure 4: Transmission spectral response to temperature.

As can be seen more than three cladding modes are excited, and the power is mainly distributed in the core mode and dominated cladding mode. The other weak cladding modes have a modulation function on the interference pattern constructed by the core mode and dominated calddding mode. The phase φ of the FMZI at the output $(z = L)$ can be expressed as,

$$\varphi \approx \frac{2\pi}{\lambda} \int_0^L [n_1 - n_2(z)] dz, \tag{1}$$

where n_1 and $n_2(z)$ are the effective refractive indexes (RIs) of the core mode and cladding mode, respectively, and $n_2(z)$ is position dependent. As the phase satisfies the condition of $\varphi = (2k+1)\pi$, where k is the interfenrence order, the reconance dip occurs. The wavelength shift $\Delta\lambda$ of the resonance dip due to temperature variation ΔT can be given by,

$$\Delta\lambda = \frac{2}{(2k+1)} [\alpha(n_1 - \overline{n_2}) + (\xi_1 - \xi_2)L] \Delta T, \tag{2}$$

where $\int_0^L n_2(z)dz = \overline{n_2}L$, $\overline{n_2}$ is the averagely effective RI of the cladding mode; $\alpha = \frac{1}{L}\frac{dL}{dT}$ is the thermal-expansion coefficient of the FMZI, $\xi_1 = \frac{1}{n_1}\frac{dn_1}{dT}$, and $\xi_2 = \frac{1}{\overline{n_2}}\frac{d\overline{n_2}}{dT}$ are the thermal-optic coefficients of the core and cladding modes, respectively. Fig. 4 shows its transmission spectral response to temperature. The transmission spectrum experiences a blue-shift as the temperature increases. Fig. 5 shows the measured relationships between the temperature and wavelength shifts of the resonance dips. There are good linear relationships between the temperature and wavelength shifts. The sensitivities of the left and right resonance dips reach 33.8 and 35.2 pm/°C.

3. MINIATURIZED FFPI AND ITS APPLICATION

Miniaturized FFPI could be fabricated by discharge using a splicer when splicing a hollow core PCF to an SMF. Here, a commercial Fujikura FSM-40PM splicer was used to fabricate the FFPI. The PCF is from NKT Photonics company, with core, pitch and cladding diameters of 10 µm ± 1 µm, 3.8 µm, and 120 µm, respectively. The cleaning arc time was set to 40 ms to avoid collapsing the core of the HCPCF, and the discharge power and time of the splicer were set to 16.29 mA and 1090 ms, respectively. Fig. 6 shows the typical microscope image of the FFPI. A thin elliptical glass layer is at the end surface of the FFPI. The length of the FFPI is about 210 µm. The maximum radial diameter of the sphere is about 180 µm. Fig. 7 shows the typical reflection spectra of the FFPI under different RI values. When the FFPI was dipped in the liquid, there is a sharp insertion loss. The reflectivity of the inner surface between the SMF and the sphere is unchanged while that of the end surface between the sphere and ambient environment is influenced by the ambiend RI. The reflectivity of the end surface can be given by $R = (\frac{n_e^- n_{amb}}{n_e^+ n_{amb}})^2$, where n_e is the effective core RI of the FPPI at the end surface, and n_{amb} is the RI of the ambient environment. The nearer of n_{amb} to n_e, the smaller R becomes.then the total reflected intensity of the FFPI decreases accordingly. Hence, the insertion loss of the FFPI will be improved as the RI of the ambient environment

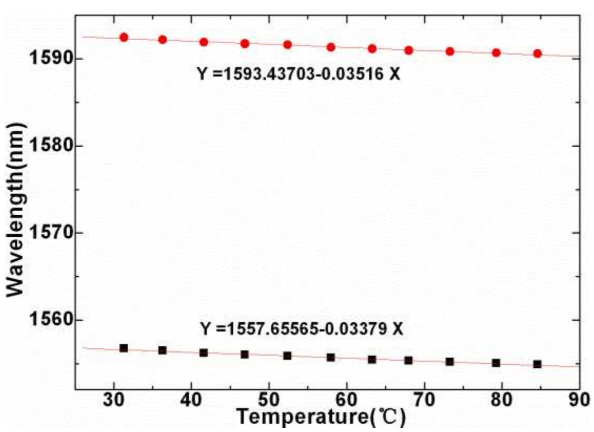

Figure 5: Relationships between the temperature and wavelength shifts of the resonance dips.

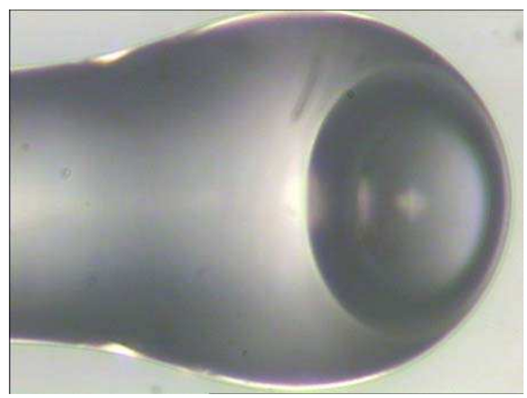

Figure 6: Typical microscope image of the FFPI.

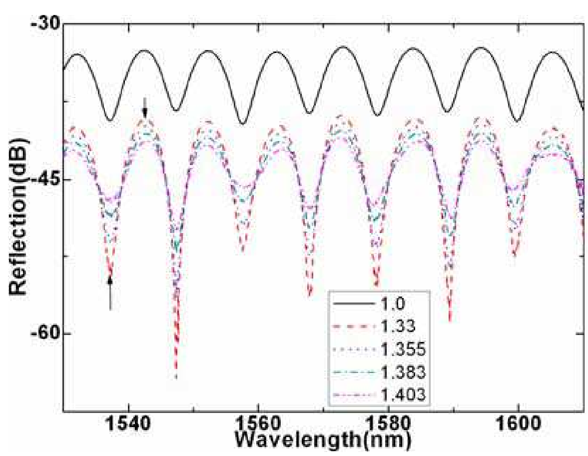

Figure 7: Typical reflection spectra of the FFPI under different RI value.

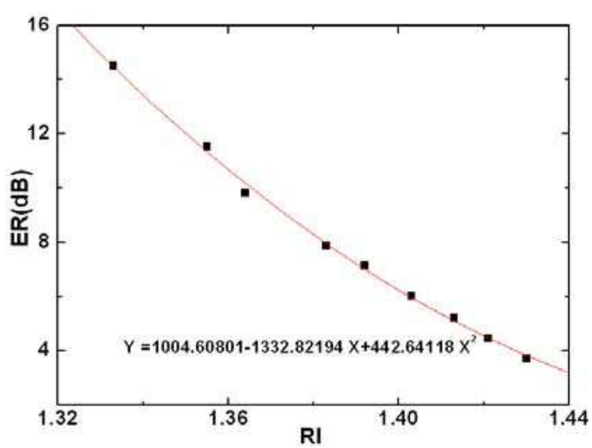

Figure 8: Reflection spectral response to RI.

increases.

Figure 8 shows the measured relationship between the RI and ER of the marked peak to dip in Fig. 7. There is a good quadratic relationship between the ER and RI. The ER changed 10.792 dB from 1.333 to 1.43. Within the RI range of 1.333 $\sim$ 1.403, there is a quasi-linear relationship between the ER and RI. A RI sensitivity of $\sim$ 120.9 dB/RI could be obtained. Under a 0.001 dB amplitude resolution, the RI resolution reaches $\sim 8.3\times10^{-6}$. It should be noted that since the FFPI has the micro-size and hollow cavity structure, it has the advantages of temperature insensitiveness and high stability.

4. CONCLUSIONS

In conclusion, two types of fiber interferometers, FMZI and FFPI, and their applications as fiber sensors were demonstrated. The FMZI could be fabricated by discharge or a point flame. As a temperature sensor, its sensitivity reached 35.2 pm/°C. The FFPI could be fabricated by discharge.As a RI sensor, its RI sensitivity reached $\sim$ 120.9 dB/RI. They are expected to have the other sensing applications, for example, the FMZI could also be use to measure the vibration, RI, strain, etc, while the FFPI could also be used to measure the pressure, vibration, etc.

ACKNOWLEDGMENT

This work is partially supported by the project of Singapore National Research Foundation with grant No. NRF2012EWT-EIRP002-044.

REFERENCES

1. Ni, K., X. Dong, C. C. Chan, T. Li, L. Hu, and W. Qian, "Miniature refractometer based on Mach-Zehnder interferometer with waist-enlarged fusion bitaper," *Opt. Commun.*, Vol. 292, 84–86, 2013.
2. Chen, N.-K., Y.-H. Hsieh, and Y.-K. Lee, "Tapered fiber Mach-Zehnder interferometers for vibration and elasticity sensing applications," *Opt. Exp.*, Vol. 21, 11209–11214, 2013.
3. Dong, B., D.-P. Zhou, L. Wei, W.-K. Liu, and J. W. Y. Lit, "Temperatureand phase-independent lateral force sensor based on a core-offset multimode fiber interferometer," *Opt. Exp.*, Vol. 16, 19291–19296, 2008.
4. Qi, F., L. Hu, X. Dong, and Y. Xin, "A hollow core fiber-based intermodal interferometer for measurement of strain and temperature," *IEEE Sensors J.*, Vol. 13, 3468–3471, 2013.
5. Dong, B. and E. J. Hao, "Core-offset hollow core photonic bandgap fiber based inter-modal interferometer for strain and temperature measurements," *Applied Optics*, Vol. 50, 2949–2957, 2011.
6. Dong, B., J. Hao, T. Zhang, and J. Lim, "High sensitive fiber-optic liquid refractive index tip sensor based on a simple inline hollow glass micro-sphere," *Sensors and Actuators B*, Vols. 171–172, 405–408, 2012.
7. Shi, Q., F. Lv, Z. Wang, L. Jin, J. Hu, Z. Liu, G. Kai, and X. Dong, "Environmentally stable Fabry-PÉrot-type strain sensor based on hollow-core photonic bandgap fiber photonics," *IEEE Photon. Tech. Lett.*, Vol. 20, 237–239, 2008.
8. Dong, B., J. Hu, Z. Chen, and C. Yu, "Long distance fiber sensor system based on the second-order Raman pump and amplification," *Applied Physics B*, Vol. 108, 57–60, 2012.
9. Dong, B., N.-K. Chen, G.-L. Cheng, C. Yu, and Y. Gong, "Optical pump induced thermal sensitivity reduction in a minimized Er/Yb-codoped-fiber Mach-Zehnder interferometer," *IEEE/OSA Journal of Lightwave Technology*, Vol. 32, No. 5, 917–921, 2014.